ACTA METALLURGICA SLOVACA
2024, VOL. 30, NO. 2, 77-89

RESEARCH PAPER

THERMODYNAMIC ANALYSIS OF PHASE DIAGRAMS BASED ON THE CONCEPT OF THE BJERRUM–GUGGENHEIM OSMOTIC COEFFICIENT

*Sailaubai Baisanov [1], Natalya Lu [1], Yelena Zhinova [1 *], Gulnara Narikbaeva [1]*

1 Zh. Abishev Chemical-Metallurgical Institute, 100009, Ermekov st. 63, Karaganda, Kazakhstan

*Corresponding author: lenuska-kar@mail.ru, tel.: +77016659763, Zh. Abishev Chemical-Metallurgical Institute, 100009, Karaganda, Kazakhstan

Received: 23.05.2024
Accepted: 29.05.2024

ABSTRACT

The aim of this study is to theoretically confirm or refute the high degree of lead and zinc volatilization from the Shalkiya deposit (polymetallic refractory ores) using analyzing the phase diagrams and the behavior of the osmotic coefficient according to the Bjerrum-Guggenheim equation along the liquidus line for binary systems based on calcium. From the plots depicting the dependence of the Bjerrum-Guggenheim osmotic coefficient on activity, one can infer the structure of the melt (positive Φ_i <1 or negative Φ_i >1). That is, if the values of the Bjerrum-Guggenheim osmotic coefficient in a binary system indicate a positive character of interaction between the components, it implies interaction between like atoms in the melt, whereas negative values indicate interaction between unlike atoms, suggesting the formation of complex, high-temperature compounds, which would be undesirable in our case. The formation of complex high-temperature chemical compounds with impurity elements such as zinc and lead in the Fe-Si-Al-Ca-Mg-Zn-Pb system remains unresolved.

Keywords: phase diagrams, congruently melting compounds, lines of monovariant phase equilibria, Bjerrum-Guggenheim osmotic coefficient

INTRODUCTION

In recent years, there has been an increasing number of publications addressing the issue of raw materials in metallurgy. The reserves of high-grade and easily processable raw materials worldwide are steadily decreasing. The forefront of research is occupied by theoretical and applied studies in the field of processing refractory polymetallic ores, particularly those from the Shalkiya deposit.

Most multi-component lead-zinc and copper-zinc ores belong to the class of refractory ores [1] – [8]. The processing of refractory polymetallic ores is characterized by its complexity due to the chemical as well as physical composition of those ores. In addition, difficulties arise due to the lack of real understanding of the phase composition of such raw materials.

MATERIAL AND METHODS

To gain insights into the behavior of zinc and lead, particularly whether complex high-temperature compounds will form in complex alloys, the main crystallization regions of binary systems based on iron, silicon, aluminum, calcium, and magnesium are mathematically described using unified analytical frameworks. The variation in the Bjerrum-Guggenheim osmotic coefficient as a function of the components' activity ratio in the ideal liquid and solid phases (positive Φ_i <1 or negative Φ_i >1) under boundary conditions governing the formation of crystallization fields of phases related to the processes of complex alloy smelting is direct evidence that zinc and lead in the melt will form volatile fractions.

In order to compute numerical values of the Bjerrum-Guggenheim osmotic coefficient and construct dependency plots (Φ_i) as a function of activity, initial data for 5 binary phase diagrams with calcium (Fe-Ca, Ca-Pb, Ca-Zn, Ca-Mg, Ca-Al, Ca-Si) have been formulated, constituting a comprehensive 7-component system of Fe-Si-Al-Ca-Mg-Zn-Pb.

All phase diagrams featuring the formation of congruently melting compounds can be divided into two groups based on their shape (radius of curvature) with sharp and low-pitched maxima. Sharp (singular) maxima of liquidus and solidus curves in both liquid and solid phases correspond to perfectly non-dissociating compounds. The radii of curvature of the liquidus lines at these points are zero. If dissociation occurs in both phases, both maxima are smooth.

We conducted a theoretical analysis of the behavior of Bjerrum-Guggenheim coefficient plots near the melting temperatures of the corresponding chemical compounds.

RESULTS AND DISCUSSION

The obtained results allow us to conclude that the proposed method is universally applicable when it comes to analytically describing phase diagrams from the perspective of the Bjerrum-Guggenheim concept [9] - [12].

The available experimental results on binary phase diagrams contain two coordinates for each point on the liquidus and solidus lines, namely: the concentration of the crystallizing component $X_i^{L(S)}$ and the temperature K.

To generate the initial data and construct the plots depicting the dependence of the Bjerrum-Guggenheim coefficient (Φ_i' и Φ_i'')

on the activity ratio in liquid and solid phases according to the Schroeder-Le Chatelier equation:

$$ln\frac{a^L_{1,id}}{a^S_{1,id}} = \frac{\Delta H_{m,i,1}}{R}\left(\frac{1}{T_{m,i,1}} - \frac{1}{T}\right) + \int_T^{T_{m,i,1}}\left[\frac{1}{RT^2}\int_T^{T_{m,i,1}}\Delta C_{p,1}dT\right]dT, \quad (1.)$$

experimental data from various model binary systems were used to obtain these values at a specific temperature T_m. according to the following equations:

$$\Phi_i = \frac{\ln(a^L_1/a^S_1)}{\ln(x^L_1/x^S_1)} \text{ and } \Phi_i = \frac{\ln(a^L_1/a^S_1)}{\ln x^L_1}, \quad (2.)$$

where x^L_1/x^S_1 is the concentration of the crystallizing component at a given temperature; a^L_1/a^S_1 is the activity of the crystallizing component for an ideal solution, calculated according to the equation (1).

The essence of the method lies in determining the Bjerrum-Guggenheim coefficient (Φ'_i и Φ''_i) along the liquidus and solidus lines in the form of dependencies listed below:

$$\Phi'_i = \ln(a^L_i/a^S_i)/(lnx^L_i/x^S_i) = (A_i{+}B_i)\,a^L_i/a^S_i, \quad (3.)$$

$$\Phi''_i = (\ln a^L_i/lna^S_i)/(\ln x^L_i = (M_i + N_i)\,a^L_i/a^S_i. \quad (4.)$$

These, in turn, made it possible to derive semi-empirical dependencies for calculating the liquidus and solidus lines of each crystallizing phase of the system under consideration:

$$lnx^L_i = \frac{\Delta H_{m,i}}{R}\left(\frac{1}{T_{m,i}} - \frac{1}{T}\right)/\Phi''_i, \quad (5.)$$

$$lnx^S_i = \frac{\Delta H_{m,i}}{R}\left(\frac{1}{T_{m,i}} - \frac{1}{T}\right)\left(\frac{1}{\Phi''_i} - \frac{1}{\Phi'_i}\right), \quad (6.)$$

where $\Delta H_{m,1(2)}$ is the melting enthalpy of the 1st and the 2nd components at the melting temperature, J/mol;
R is the universal gas constant, 8.3144 J/mol K;
$T_{m,1(2)}$ is the melting temperature of the 1st and the 2nd components and crystallization of the melts, K;
T is the current temperature along the liquidus line, K;
Φ'_i is the Bjerrum-Guggenheim coefficient for the 1st and the 2nd components, which allows one to find the correlation dependence and obtain a mathematical expression for the ratio of activities of the i[th] component in the liquid and solid phases according to equation (3);
Φ''_i is the Bjerrum-Guggenheim coefficient for the 1st and the 2nd components, which allows one to find the correlation dependence and obtain a mathematical expression for the liquidus line of the i[th] component according to equation (4).

For the dependencies (3, 4), the equation coefficients are computed using the method of least squares, with the establishment of the correlation coefficient R_{xy} (for linear dependencies) or through the convergence dispersion σ (for nonlinear dependencies). All calculations are performed using programs written in the Delphi language. With the programs developed by us, phase equilibria of numerous binary systems were studied.

Processing the obtained results using the method of least squares allows to find the values of constants and correlation coefficients for various systems and deriving analytical expressions for phase crystallization fields for any quasi-system (for the partial system).

In addition, based on the real possibility of assessing the behavior of compounds in the melt and the nature of interparticle interactions in the liquid phase using the Bjerrum-Guggenheim osmotic coefficient (Φ_i), the analysis of the phase crystallization lines also allows for determining the reliability of data on the phase diagrams of these systems and the stability of the compounds in the melts.

This methodology enables thermodynamic assessment of the mutual solubility of components in each other based on the nature of the change in the Bjerrum-Guggenheim osmotic coefficient.

1. Ca – Pb phase diagram

There are four intermetallic compounds in the system, two of which, CaPb3 and Ca2Pb, melt congruently at 666 and 12050C, respectively. CaPb and Ca5Pb3 compounds are formed by peritectic reactions at 908 and 1127^{0}C, respectively (**Fig. 1**).

The reference data from [13] generated initial data on simple and complex components' enthalpies and melting temperatures. The enthalpies of substances for which data could not be found were calculated.

Four crystallization areas were considered in this system, i.e. two for the partial systems Pb_3Ca-Pb and Pb_3Ca-Ca, and two partial systems for the relatively congruent compound Ca_2Pb: Ca_2Pb-Pb Ca_2Pb-Ca.

The first Pb3Ca crystallization region in the Pb3Ca-Pb system (**Fig. 1**) is quite extensive. It starts from the melting point of Pb3Ca (939 K) and goes through to the melting temperature of lead (600 K) [14] - [19].

The procedure for mathematical description of monovariant phase equilibrium lines on the phase diagram based on the concept of the Bjerrum-Guggenheim osmotic coefficient is described in [9] - [12]. For thermodynamic calculations, the enthalpy of melting was assumed to be equal to $\Delta H_{m,CaPb3}$ == 7450 J/mol at a melting temperature of 939 K [14], [15], [19].

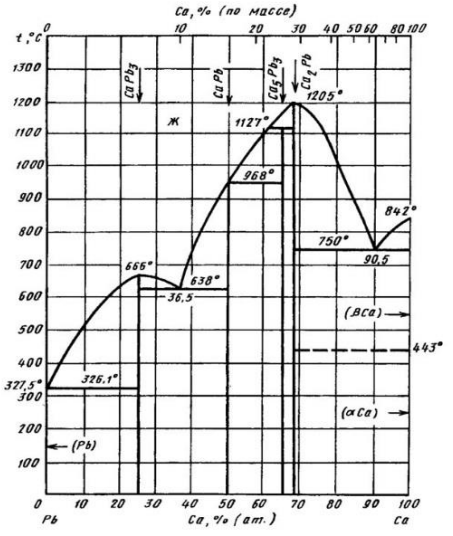

Fig. 1 Ca-Pb phase diagram

Table 1 presents the initial data on the crystallization of Pb_3Ca by temperature and its corresponding composition up to the eutectic line at 1588 K.

Table 1 Initial data for the Pb_3Ca crystallization region in the Pb-Ca system

T,K	x^L_{Pb}	x^S_{Pb}	$x^L_{Pb_3Ca_{изотерм.}}$	$\ln a^L_{CaPb_3}$	$a^L_{CaPb_3}$	$\Phi'_{Pb_{оп.}}$	$\Phi'_{CaPb_{3оп.}}$
939	0,75	0,75	1	0	1	0	0
933	0,775	0,75	0,692308	-0,00614	0,993882	0,024076	0,016688
898	0,815	0,75	0,41573	-0,04357	0,957367	0,212979	0,049638
873	0,832	0,75	0,33871	-0,07214	0,930398	0,392246	0,066638
848	0,85	0,75	0,272727	-0,1024	0,902666	0,630096	0,078815
823	0,87	0,75	0,213115	-0,1345	0,874153	0,965807	0,087003
798	0,886	0,75	0,173252	-0,16861	0,844839	1,393023	0,096183
748	0,92	0,75	0,105263	-0,24367	0,783749	2,922311	0,108234
723	0,936	0,75	0,079208	-0,28509	0,751947	4,3104	0,112431
698	0,95	0,75	0,058824	-0,32948	0,719299	6,423416	0,116291
673	0,963	0,75	0,04162	-0,37717	0,685803	10,00389	0,118636
648	0,973	0,75	0,02938	-0,42853	0,651465	15,6563	0,121485
623	0,981	0,75	0,020148	-0,48402	0,6163	25,23199	0,123961
600,5	0,987	0,75	0,013528	-0,53791	0,583967	41,10825	0,125008

Now, we plot the dependence of $\Phi''_{оп}$ on $a^L_{Pb_3Ca}$ for the base system (**Fig. 2**) in order to see the behavior of the components in the melt.

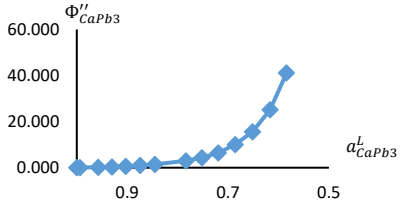

Fig. 2 Dependence of the Bjerrum-Guggenheim osmotic coefficient $\Phi''_{оп}$ on the activity ratio $a^L_{Pb_3Ca} / a^S_{Pb_3Ca}$

The graph exhibits a distinctly nonlinear relationship, indicating strong positive deviations from ideality. Upon recalculating the initial data by composition for the partial Pb_3Ca-Pb system using equation (7)

x1= (Q1–(Q1+P1).x0)/((I1+J1–Q1–P1).x0–I1+Q1) (7.)

new data on the composition were obtained and they are in the columns x^L_{Pb} and x^S_{Pb} of the **Table 1**. Conversion factors for the partial Pb_3Ca-Pb system are given as follows I=3, J=1, Q=1, P=0.

We constructed a new plot of the dependence of the Bjerrum-Guggenheim osmotic coefficient for a partial system (**Fig. 3**).

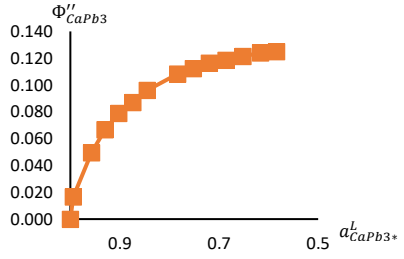

Fig. 3 Dependence of the Bjerrum-Guggenheim osmotic coefficient (Φ''_{CaPb3}) on activity $a^L_{CaPb_3}$ for the partial Pb_3Ca-Pb system

The Φ''_{CaPb3} versus a^L_{CaPb3*} plot (**Fig. 3**) is convex, which means that the process of dissociation of the congruent compound occurs in the melt. It sharply increases with the melting temperature of Pb_3Ca, and then dissociation proceeds more smoothly (8):

$$\Phi''_{расч} = 1{,}4305 - 0{,}9758 \cdot a^L_{CaPb_3} + 0{,}4352/(0 - a^S_{CaPb_3}),(8.)$$

The mathematical expression of the Pb_3Ca crystallization line in the Pb_3Ca-Pb system is given in the form of a semi-empirical dependence of the Schroeder-Le Chatelier equation (9):

$$lnx^L_{CaPb_3} = \frac{\frac{7450}{8{,}3143}\left(\frac{1}{939}-\frac{1}{T}\right)+\int_T^{T_{m,i}}\left[\frac{1}{RT^2}\int_T^{T_{m,i}}\Delta C_p dT\right]dT}{1{,}4305-0{,}9758+0{,}4352\cdot exp\left[\frac{7450}{8{,}3143}\left(\frac{1}{939}-\frac{1}{T}\right)+\int_T^{T_{m,i}}\left[\frac{1}{RT^2}\int_T^{T_{m,i}}\Delta C_p dT\right]dT\right]}, \quad (9.)$$

Table 2 shows the results on the convergence of the calculated (9) and experimental data (Table 1) obtained.

Table 2 Comparative analysis of the calculated and experimental data for the Pb_3Ca crystallization region in the Pb_3Ca-Pb system

$\Phi'_{CaPb_{3эл.}}$	$\Phi'_{CaPb_{3расч.}}$	$a^L_{CaPb_3}$	$\ln a^L_{CaPb_3}$	$x^L_{CaPb_{3э.с.эл.}}$	$x^L_{CaPb_{3э.с.расч.}}$
0	0,0195	1	0	1	1
0,016688	0,022791	0,993882	-0,00613679	0,692308	0,763942
0,049638	0,04172117	0,957367	-0,04356847	0,41573	0,351946
0,066638	0,05486082	0,930398	-0,07214283	0,33871	0,26847
0,078815	0,06755113	0,902666	-0,10240267	0,272727	0,219604
0,087003	0,07964815	0,874153	-0,13449986	0,213115	0,184764
0,096183	0,09097837	0,844839	-0,1686092	0,173252	0,156721
0,108234	0,11043791	0,783749	-0,24366646	0,105263	0,1101
0,112431	0,11798592	0,751947	-0,28508944	0,079208	0,089251
0,116291	0,12357452	0,719299	-0,32947815	0,058824	0,069514
0,118636	0,12670887	0,685803	-0,37716486	0,04162	0,050965
0,121485	0,12676763	0,651465	-0,42853161	0,02938	0,034032
0,123961	0,12296486	0,6163	-0,48402142	0,020148	0,019521
0,125008	0,11541741	0,583967	-0,5379108	0,013528	0,009461

We will now consider the Pb_3Ca crystallization region for the partial Pb_3Ca-Ca system. We conducted the same manipulations as in the first area. We collected data on the phase diagram (**Fig. 1**) for temperatures ranging from 939 through to 911 K and the corresponding composition. The initial data is presented in **Table 3**. For thermodynamic calculations, the melting enthalpy was assumed to be equal to ΔH_{mCaPb3} = 7450 J/mol [13], [14], [15] at a melting temperature of 939 K [8].

Table 3 Initial data of the Pb_3Ca crystallization region for the partial Pb_3Ca-Ca system

T,K	x^L_{Pb}	x^S_{Pb}	$x^L_{Pb_3Ca_{часм.}}$	$\ln a^L_{CaPb_3}$	$a^L_{CaPb_3}$	$\Phi'_{Pb_{эл.}}$
939	0,75	0,75	1	1	0	0
931	0,685	0,75	0,724868	0,991834	0,021674	0,025484
923	0,674	0,75	0,689162	0,983594	0,041929	0,044434
915	0,656	0,75	0,635659	0,975281	0,05937	0,055242
911	0,645	0,75	0,605634	0,971096	0,066886	0,058487

The dependence of the osmotic coefficient $\Phi''_{оп}$ on the activity $a^L_{CaPb_3}$ of the component for the ideal state is graphically presented in **Fig. 4**.

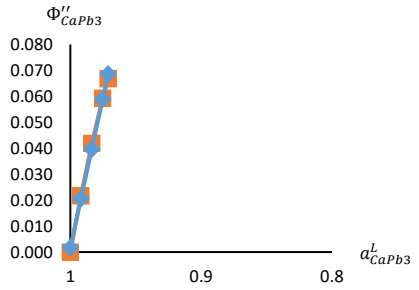

Fig. 4 The graph of the dependence of the Bjerrum-Guggenheim osmotic coefficient $\Phi''_{оп}$ on the Pb_3Ca crystallization activity $a^L_{CaPb_3}$ of the partial Pb_3Ca-Ca system

What is characteristic of this particular Pb_3Ca crystallization region? The graph exhibits a strictly correlated relationship with a correlation coefficient of -0.998:

$$\Phi''_{расч} = 2{,}319 - 2{,}318 \cdot a^L_{CaPb_3},\ R_{xy} = -\,0{,}998 \qquad (10.)$$

relative to the basic Pb-Ca system. This means that this Pb_3Ca crystallization region is characterized by the presence of van der Waals interaction forces between the components.

Using the Schroeder-Le Chatelier equation for an ideal system (9) and equation (10), which characterizes the deviation of the properties of a real system from an ideal one, we obtained the calculated values of the x^L components according to the mathematical relationship (11):

$$lnx^L_{CaPb_3} = \frac{\frac{7450}{8{,}3143}\left(\frac{1}{939}-\frac{1}{T}\right)+\int_T^{Tm,i}\left[\frac{1}{RT^2}\int_T^{Tm,i}\Delta C_p dT\right]dT}{2{,}319-2{,}318\cdot exp\left[\frac{7450}{8{,}3143}\left(\frac{1}{939}-\frac{1}{T}\right)+\int_T^{Tm,i}\left[\frac{1}{RT^2}\int_T^{Tm,i}\Delta C_p dT\right]dT\right]}, \qquad (11.)$$

Then, the obtained results (11) were compared with the experimental values in **Table 3**. The experimental and calculated data are given in **Table 4**.

Table 4 Comparative analysis of the calculated and experimental data for the Pb_3Ca crystallization region in the Pb_3Ca-Ca system

$\Phi'_{CaPb_{3эк.}}$	$\Phi'_{CaPb_{3расч.}}$	$a^L_{CaPb_3}$	$\ln a^L_{CaPb_3}$	$x^L_{CaPb_{3ч.с.эк.}}$	$x^L_{CaPb_{3ч.с.расч.}}$
0	0,0017	1	0	0,75	1
0,021674	0,020626	0,991834	-0,00819952	0,685	0,671969
0,041929	0,039723	0,983594	-0,01654207	0,674	0,65939
0,05937	0,058989	0,975281	-0,02502964	0,656	0,65422
0,066886	0,068688	0,971096	-0,02932995	0,645	0,652462

The conclusion regarding the congruent compound Pb_3Ca crystallization region for the two partial systems, i.e. Pb_3Ca-Pb and Pb_3Ca-Ca, is as follows: from the lead side of the Pb_3Ca-Pb partial system, dissociation of the compound predominantly occurs (the Bjerrum-Guggenheim coefficient exhibits a positive deviation from ideality), and the degree of dissociation increases as the temperature changes further. On the other hand, considering the calcium side of the Pb_3Ca crystallization region, van der Waals forces predominantly govern the interactions between the components.

We will now consider the high-temperature congruent compound Ca_2Pb crystallization region. For thermodynamic calculations, we adopted the enthalpy of fusion as H_{mCa2Pb} = 12400 J/mol [14] at the melting temperature of 1478 K [19]. Similar to obtaining data on the melt structure in the Ca_2Pb crystallization region, we collected initial data from the phase diagram (**Fig. 1**) for the temperature range of 1478-911 K and the corresponding composition. The initial data are presented in **Table 5**.

A graph (**Fig. 5**) depicting the dependence of the Bjerrum-Guggenheim coefficient on activity was constructed for the baseline data (without conversion to the formation of Ca2Pb). It is visually apparent that the graph exhibits a nonlinear relationship, indicating either the formation of associates of varying complexity in accordance with the compounds present on the diagram, or dissociation of the compound, or the formation of dimers, trimers, etc. in the crystallization region of pure elements. Additionally, the values of the Bjerrum-Guggenheim coefficient from activity are less than one, indicating interaction between like atoms in the melt, hence an intense dissociation process is occurring.

Table 5 Initial data on the Ca_2Pb crystallization region of the Ca – Pb system

T,K	x^L_{Pb}	x^S_{Pb}	$x^L_{Ca_2Pb_{исслед.}}$	$\ln a^L_{Ca_2Pb}$	$a^L_{Ca_2Pb}$	$\Phi'_{Pb_{эк.}}$
1478	0,333	0,333	1,001502	1	0	0
1448	0,346	0,333	0,945087	0,975685	0,023193	0,435834
1423	0,349	0,333	0,932665	0,955117	0,043623	0,658747
1398	0,352	0,333	0,920455	0,934271	0,065115	0,820249
1373	0,4	0,333	0,75	0,913146	0,09916	0,315834
1348	0,419	0,333	0,693317	0,891741	0,131718	0,31283
1323	0,44	0,333	0,636364	0,870058	0,169548	0,307964
1298	0,46	0,333	0,586957	0,848098	0,212174	0,309231
1273	0,478	0,333	0,546025	0,825862	0,259201	0,316197
1248	0,49	0,333	0,520408	0,803353	0,306947	0,335242
1241	0,5	0,333	0,5	0,797003	0,327344	0,327344
1198	0,519	0,333	0,463391	0,757535	0,423398	0,361014
1173	0,53	0,333	0,443396	0,734235	0,486591	0,379847
1148	0,547	0,333	0,414077	0,710684	0,566092	0,387349
1123	0,57	0,333	0,377193	0,686891	0,668149	0,38521
1098	0,58	0,333	0,362069	0,662866	0,75484	0,404738
1073	0,589	0,333	0,348896	0,638621	0,847193	0,425881
1048	0,591	0,333	0,346024	0,61417	0,926882	0,459349
1023	0,599	0,333	0,334725	0,589529	1,031098	0,482829
998	0,6	0,333	0,333333	0,564717	1,118641	0,520138
973	0,61	0,333	0,319672	0,539755	1,24751	0,540694
948	0,619	0,333	0,307754	0,514668	1,384828	0,563648
911	0,625	0,333	0,3	0,477369	1,573317	0,614187

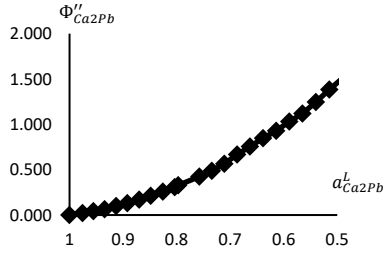

Fig. 5 Graph of the dependence of the Bjerrum-Guggenheim osmotic coefficient $\Phi''_{оп}$ on the Ca_2Pb crystallization activity a^L_{Ca2Pb} of the baseline Ca - Pb system

In order to obtain the mathematical dependence of the Bjerrum-Guggenheim osmotic coefficient on activity, the least squares method was employed (12):

$$\Phi'' = -1{,}581 + 0{,}0281 \cdot a^L_{Ca_2Pb} \text{-} 1{,}517/(0\text{-}a^S_{Ca_2Pb}),\ \sigma = -0.013 \quad (12.)$$

The mathematical expression of the Ca_2Pb crystallization line in the Ca_2Pb - Pb system is given in the form of a semi-empirical dependence of the Schroeder-Le Chatelier equation (13):

$$ln x^L_{Ca_2Pb} = \frac{\frac{14600}{8{,}3143}\left(\frac{1}{1478}-\frac{1}{T}\right)+\int_T^{Tm,i}\left[\frac{1}{RT^2}\int_T^{Tm,i}\Delta C_p dT\right]dT}{-1{,}581+0{,}0281-1{,}517\cdot exp\left[\frac{14600}{8{,}3143}\left(\frac{1}{1478}-\frac{1}{T}\right)+\int_T^{Tm,i}\left[\frac{1}{RT^2}\int_T^{Tm,i}\Delta C_p dT\right]dT\right]} \quad (13.)$$

According to (12) and (13), a comparative analysis of the convergence of the calculated and experimental data was conducted and its results are listed in **Table 6**.

Table 6 Comparative analysis of the calculated and experimental data for the Ca_2Pb crystallization region in the Ca_2Pb – Pb system

T, K	$\Phi^{'}_{Ca_2Pb_{оп.}}$	$\Phi^{'}_{Ca_2Pb_{расч.}}$	$a^L_{Ca_2Pb}$	$\ln a^L_{Ca_2Pb}$	$x^L_{Ca_2Pb_{к.с.оп.}}$	$x^L_{Ca_2Pb_{к.с.расч.}}$
1478	0	-0,0359	1	0	0,333	1
1448	0,023193	0,001222	0,975685	-0,02461549	0,346	1,78E-09
1423	0,043623	0,034126	0,955117	-0,04592143	0,349	0,260371
1398	0,065115	0,068979	0,934271	-0,06798873	0,352	0,373198
1373	0,09916	0,105949	0,913146	-0,0908595	0,4	0,424189
1348	0,131718	0,145225	0,891741	-0,11457955	0,419	0,454307
1323	0,169548	0,187011	0,870058	-0,1391954	0,44	0,475058
1298	0,212174	0,23154	0,848098	-0,16475908	0,46	0,490868
1273	0,259201	0,279075	0,825862	-0,19132759	0,478	0,5038
1248	0,306947	0,32991	0,803353	-0,21896106	0,49	0,514943
1241	0,327344	0,344776	0,797003	-0,22689684	0,5	0,517835
1198	0,423398	0,442834	0,757535	-0,27768554	0,519	0,534158
1173	0,486591	0,505728	0,734235	-0,30892614	0,53	0,542887
1148	0,566092	0,573534	0,710684	-0,34152739	0,547	0,551298
1123	0,668149	0,646803	0,686891	-0,37557966	0,57	0,559523
1098	0,75484	0,726174	0,662866	-0,41118242	0,58	0,567661
1073	0,847193	0,812376	0,638621	-0,44844411	0,589	0,575788
1048	0,926882	0,906258	0,61417	-0,48748352	0,591	0,583969
1023	1,031098	1,008806	0,589529	-0,52843137	0,599	0,592255
998	1,118641	1,12117	0,564717	-0,57143056	0,6	0,600692
973	1,24751	1,244702	0,539755	-0,61663995	0,61	0,60932
948	1,384828	1,380993	0,514668	-0,66423325	0,619	0,618176
911	1,573317	1,610249	0,477369	-0,7394655	0,625	0,631774

The first noticeable observation when analyzing the convergence of the experimental and calculated compositions is the lack of convergence from the melting temperature of Ca_2Pb up to 1241 K. Within this temperature range, the formation of the incongruent Ca_5Pb_3 and CaPb compounds occurs, indicating their strong influence on the congruent Ca_2Pb compound's formation.

We constructed a graph showing the dependence of the Bjerrum-Guggenheim osmotic coefficient $\Phi''_{оп}$ on activity for the partial Ca_2Pb-Pb system (**Fig. 6**). The calculated compositions adjusted for the formation of the congruent Ca_2Pb compound are provided in **Table 5**.

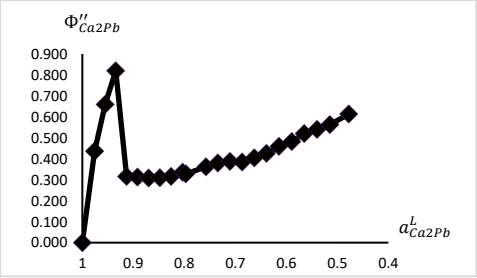

Fig. 6 Graph of the dependence of the Bjerrum-Guggenheim osmotic coefficient $\Phi''_{оп}$ on the Ca_2Pb crystallization activity a^L_{Ca2Pb} of the partial Ca_2Pb – Pb system

From the melting temperature of 1478 K to the formation of the first incongruent Ca_5Pb_3 compound, the graph experiences a sharp surge, and little can be done about it. According to the calculated data, the influence of the second incongruent CaPb compound on the graph's position is not significant but still considerable.

Given the substantial impact of incongruent compounds, we recalculated the data to account for their formation and observed how the graph of the Bjerrum-Guggenheim osmotic coefficient would change. **Table 7** shows the composition of Ca_2Pb considering the formation of Ca_5Pb_3 and CaPb.

It's worth noting that Table 7 provides data for the Bjerrum-Guggenheim osmotic coefficient for the baseline system Φ''. Negative values of the coefficient from the melting temperature up to the eutectic point only increase. The curvature of Φi is primarily influenced by the nature of the directional bonds in the associates and the change in their numerical values with temperature, as well as the degree of dissociation of the compound or its stabilization, even transitioning smoothly to association processes as the temperature changes further.

Fig. 7 shows a graph of the dependence of the Bjerrum-Guggenheim osmotic coefficient ($\Phi''_{оп}$) on the activity of Ca_2Pb crystallization of the private Ca_2Pb – Pb system, taking into account the formation of incongruent compounds Ca_5Pb_3 and CaPb. As we can see from the picture, it has become strictly linear.

Table 7 Initial data for the Ca_2Pb crystallization region for the Ca_2Pb – Pb system, taking into account the formation of incongruent compounds Ca_5Pb_3 and CaPb

T, K	x^L_{Ca}	x^S_{Ca}	$x^L_{Ca_{част.}}$	$a^L_{Ca_2Pb}$	$\Phi'_{Ca_2Pb_{баз.}}$	$\Phi'_{Ca_2Pb_{ч.с.}}$
1478	0,333	0,333	1,002	1	0	0
1448	0,49	0,333	0,520	0,975685	-0,06373	0,037601
1423	0,5	0,333	0,500	0,955117	-0,11298	0,066107
1398	0,51	0,333	0,480	0,934271	-0,1595	0,092545
1373	0,512	0,333	0,477	0,913146	-0,21121	0,122344
1348	0,514	0,333	0,473	0,891741	-0,26396	0,152638
1323	0,518	0,333	0,465	0,870058	-0,31504	0,181556
1298	0,523	0,333	0,456	0,848098	-0,36497	0,209428
1273	0,528	0,333	0,447	0,825862	-0,41507	0,237154
1248	0,532	0,333	0,440	0,803353	-0,46736	0,266109
1241	0,53	0,333	0,443	0,797003	-0,48823	0,278473
1198	0,538	0,333	0,429	0,757535	-0,57885	0,327869
1173	0,543	0,333	0,421	0,734235	-0,63179	0,356286
1148	0,55	0,333	0,409	0,710684	-0,68064	0,381459
1123	0,56	0,333	0,393	0,686891	-0,72255	0,401341
1098	0,57	0,333	0,377	0,662866	-0,765	0,421078
1073	0,573	0,333	0,373	0,638621	-0,82625	0,453547
1048	0,58	0,333	0,362	0,61417	-0,87853	0,479136
1023	0,586	0,333	0,353	0,589529	-0,93498	0,507082
998	0,59	0,333	0,347	0,564717	-0,99904	0,539792
973	0,6	0,333	0,333	0,539755	-1,0473	0,560524
948	0,608	0,333	0,322	0,514668	-1,10332	0,58597
911	0,62	0,333	0,306	0,477369	-1,18966	0,624445

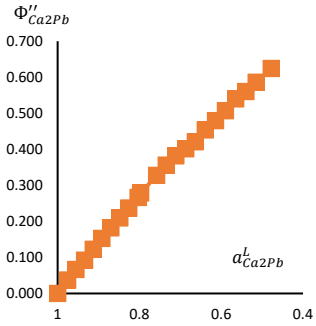

Fig. 7 Graph of the dependence of the Bjerrum-Guggenheim osmotic coefficient (Φ''_{on}) on the activity $a^L_{Ca_2Pb}$ crystallization of Ca_2Pb of the private system Ca_2Pb - Pb, taking into account the formation of incongruent compounds Ca_5Pb_3 and CaPb

Equation of mathematical dependence for the Bjerrum-Guggenheim osmotic coefficient (F_op^") on activity (14)

$$\Phi''_{\text{расч}} = 1.2104 - 1{,}1879 a^L_{CaPb_3},\ R_{xy} = -0{,}9982 \qquad (14.)$$

Using the Schroeder-Le Chatelier equation for an ideal system and equation (14), which characterizes the deviation of the properties of a real system from an ideal one, we obtained the calculated values of the components X^L and X^S according to the mathematical relationship (15):

$$lnx^L_{Ca_2Pb} = \frac{\frac{14600}{8{,}3143}\left(\frac{1}{1478}-\frac{1}{T}\right)+\int_T^{T_{m,i}}\left[\frac{1}{RT^2}\int_T^{T_{m,i}}\Delta C_p dT\right]dT}{1{,}2104-1{,}1879\cdot exp\left[\frac{14600}{8{,}3143}\left(\frac{1}{1478}-\frac{1}{T}\right)+\int_T^{T_{m,i}}\left[\frac{1}{RT^2}\int_T^{T_{m,i}}\Delta C_p dT\right]dT\right]} \qquad (15.)$$

Then the results obtained using (15) were compared with the experimental values. Experimental and calculated data are given in **Table 8**.

Table 8 Comparative analysis of the calculated and experimental data for the Ca_2Pb crystallization region of the partial Ca_2Pb-Pb system, taking into account the formation of incongruent Ca_5Pb_3 and CaPb compounds

$\Phi'_{Ca_2Pb_{on.}}$	$\Phi'_{Ca_2Pb_{расч.}}$	$a^L_{Ca_2Pb}$	$\ln a^L_{Ca_2Pb}$	$x^L_{Ca_2Pb_{э.с.эк.}}$	$x^L_{Ca_2Pb_{э.с.расч.}}$
0	0,0225	0	1	1,002	1,0000
0,037601	0,0514	-0,02462	0,975685	0,520	0,6193
0,066107	0,0758	-0,04592	0,955117	0,500	0,5457
0,092545	0,1006	-0,06799	0,934271	0,480	0,5087
0,122344	0,1257	-0,09086	0,913146	0,477	0,4853
0,152638	0,1511	-0,11458	0,891741	0,473	0,4685
0,181556	0,1769	-0,1392	0,870058	0,465	0,4552
0,209428	0,2029	-0,16476	0,848098	0,456	0,4440
0,237154	0,2294	-0,19133	0,825862	0,447	0,4342
0,266109	0,2561	-0,21896	0,803353	0,440	0,4253
0,278473	0,2636	-0,2269	0,797003	0,443	0,4229
0,327869	0,3105	-0,27769	0,757535	0,429	0,4089
0,356286	0,3382	-0,30893	0,734235	0,421	0,4011
0,381459	0,3662	-0,34153	0,710684	0,409	0,3935
0,401341	0,3944	-0,37558	0,686891	0,393	0,3859
0,421078	0,4230	-0,41118	0,662866	0,377	0,3783
0,453547	0,4518	-0,44844	0,638621	0,373	0,3706
0,479136	0,4808	-0,48748	0,61417	0,362	0,3628
0,507082	0,5101	-0,52843	0,589529	0,353	0,3549
0,539792	0,5396	-0,57143	0,564717	0,347	0,3468
0,560524	0,5692	-0,61664	0,539755	0,333	0,3385
0,58597	0,5990	-0,66423	0,514668	0,322	0,3299
0,624445	0,6433	-0,73946	0,477369	0,306	0,3168

Next, we processed the Ca_2Pb crystallization area for the partial Ca_2Pb-Ca system. We also took the initial data on the melting point and the corresponding composition. The initial data is shown in **Table 9**.

Table 9 Initial data on the Ca_2Pb crystallization region for the partial Ca_2Pb-Ca system

T, K	x^L_{Ca}	x^S_{Ca}	$x^L_{Ca_{isocon.}}$	$a^L_{Ca_2Pb}$	$\Phi'_{Ca_2Pb_{isocon.}}$	$\Phi'_{Ca_2Pb_{s.c.}}$
1478	0,667	0,667	0,997006	1	0	0
1448	0,73	0,667	0,541667	0,975685	0,078216	0,040149
1423	0,75	0,667	0,5	0,955117	0,159624	0,06625
1398	0,758	0,667	0,468992	0,934271	0,245382	0,089793
1373	0,77	0,667	0,44697	0,913146	0,347636	0,112832
1348	0,772	0,667	0,419118	0,891741	0,442783	0,13176
1323	0,781	0,667	0,38968	0,870058	0,563133	0,147698
1298	0,79	0,667	0,368056	0,848098	0,698956	0,164838
1273	0,8	0,667	0,344595	0,825862	0,85742	0,179585
1248	0,81	0,667	0,316993	0,803353	1,039102	0,190587
1223	0,82	0,667	0,293651	0,780576	1,248284	0,202163
1198	0,835	0,667	0,273994	0,757535	1,539932	0,214487
1173	0,85	0,667	0,253012	0,734235	1,900862	0,224785
1148	0,86	0,667	0,230994	0,710684	2,264423	0,233066
1123	0,87	0,667	0,210227	0,686891	2,696923	0,240823
1098	0,88	0,667	0,188705	0,662866	3,216546	0,246576
1073	0,89	0,667	0,166667	0,638621	3,848186	0,250281
1023	0,9	0,667	0,125	0,589529	5,015458	0,254122

Using the values of Φ'_{Ca_2Pb} and $a^L_{Ca_2Pb}$ from the table for the partial Ca_2Pb-Ca system, we plotted the dependence of the osmotic coefficient on the activity ratio (**Fig. 8**).
The resulting graph in **Fig. 8** is clearly convex, which means that an intense dissociation of the congruent Ca_2Pb compound occurs in the melt.

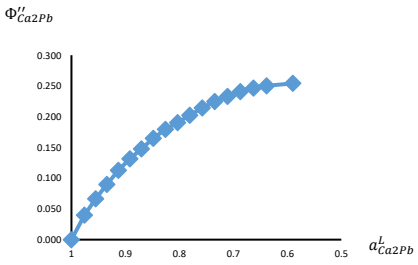

Fig. 8 Graph of the dependence of the Bjerrum-Guggenheim osmotic coefficient (Φ''_{on}) on the Ca_2Pb crystallization activity $a^L_{Ca_2Pb}$ for the partial Ca_2Pb – Ca system

The calculated osmotic coefficient values for a nonlinear relationship were found using the least squares method in the form of equation (16):

$$\Phi''_{Ca_2Pb} = 2{,}554 - 1{,}8004 \cdot a^L_{Ca_2Pb} + 0{,}7359/(0\text{-}a^S_{Ca_2Pb}),$$
$$\sigma = 0.0097, \quad (16.)$$

The mathematical expression of the Ca_2Pb crystallization line in the Ca_2Pb-Ca system is given in the form of a semi-empirical dependence of the Schroeder-Le Chatelier equation (17).

$$ln x^L_{Ca_2Pb} = \frac{\frac{14600}{8{,}3143}\left(\frac{1}{1478}-\frac{1}{T}\right)+\int_T^{Tm,i}\left[\frac{1}{RT^2}\int_T^{Tm,i}\Delta C_p dT\right]dT}{2{,}554-1{,}8004+0{,}7359\cdot exp\left[\frac{14600}{8{,}3143}\left(\frac{1}{1478}-\frac{1}{T}\right)+\int_T^{Tm,i}\left[\frac{1}{RT^2}\int_T^{Tm,i}\Delta C_p dT\right]dT\right]}, \quad (17.)$$

According to the obtained results, the equations (17) with experimental values (**Table 9**) were used to analyze the convergence of calculated and experimental data. The results are presented in **Table 10**.

Table 10 Comparative analysis of the calculated and experimental data for the Ca_2Pb crystallization region in the partial Ca_2Pb-Ca system

$\Phi'_{Ca_2Pb_{on.}}$	$\Phi'_{Ca_2Pb_{pacv.}}$	$a^L_{Ca_2Pb}$	$\ln a^L_{Ca_2Pb}$	$x^L_{Ca_2Pb_{k.c.on.}}$	$x^L_{Ca_2Pb_{k.c.pacv.}}$
0	0,018	1	0	0,997006	1
0,040144	0,0434251	0,975685	-0,0246154	0,541667	0,567311
0,066253	0,06420318	0,955117	-0,0459214	0,5	0,489069
0,089794	0,0845322	0,934271	-0,0679887	0,468992	0,447404
0,112838	0,1043324	0,913146	-0,0908595	0,44697	0,418589
0,131766	0,12351444	0,891741	-0,11457955	0,419118	0,395478
0,147698	0,14197498	0,870058	-0,1391954	0,38968	0,375153
0,164838	0,15959936	0,848098	-0,16475908	0,368056	0,356176
0,179585	0,17625835	0,825862	-0,19132759	0,344595	0,337734
0,190587	0,19180446	0,803353	-0,21896106	0,316993	0,319313
0,202163	0,20606975	0,780576	-0,24772317	0,293651	0,300553
0,214487	0,21886473	0,757535	-0,27768554	0,273994	0,281182
0,224785	0,22997314	0,734235	-0,30892614	0,253012	0,260979
0,233066	0,23914678	0,710684	-0,34152739	0,230994	0,239762
0,240823	0,2461016	0,686891	-0,37557966	0,210227	0,217378
0,246576	0,25051121	0,662866	-0,41118242	0,188705	0,193714
0,250281	0,25199896	0,638621	-0,44844411	0,166667	0,168714
0,254122	0,24439353	0,589529	-0,52843137	0,125	0,11507

The conclusions regarding the crystallization region of the Ca_2Pb-Pb and Ca_2Pb-Ca partial systems are as follows: the structure of the melt is not as simple as it seems at the first glance. Graphs of the dependence of the Bjerrum-Guggenheim osmotic coefficient (Φ'_{Ca_2Pb}) on the Ca_2Pb crystallization activity a^L_{Ca2Pb} for the partial Ca_2Pb–Pb and Ca_2Pb–Ca systems even in terms of partial systems clearly demonstrate a nonlinear character. This indicates that besides the high-temperature congruent compound, the melt also contains and is strongly influenced by the presence of incongruent Ca_5Pb_3 and CaPb compounds [20], [21]. Negative deviations of the osmotic coefficient from the ideal state further confirm the possibility of forming associations of varying complexity in the melt.

2. Ca – Zn phase diagram

The system (**Fig. 9**) exhibits the formation of eight compounds. The compounds $CaZn_2$ (76.53% (by mass) Zn), $CaZn_5$ (89.08% (by mass) Zn), CaZn, (94.72% (by mass) Zn) melt at temperatures of 704, 695 and 724°C, respectively. Compounds Ca_3Zn (35.22% (by mass) Zn), Ca_5Zn_3 (48.24% (by mass) Zn), CaZn (62.0% (by mass) Zn), $CaZn_3$ (82.33% (by mass) Zn) Zn) and $CaZnI_3$ (95.5% (by mass) Zn) are formed by peritectic reactions at temperatures of 394, 414, 439, 642 and 669°C, respectively. Three eutectic transformations occur in the system at temperatures of 391, 638, 690°C and contents of 27.4, 76.4 and 86.7% (at.) Zn. The mutual solubility of Ca and Zn in the solid state has not been established [13].

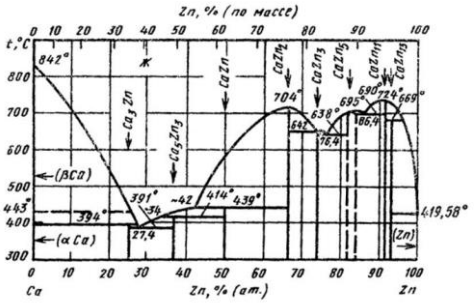

Fig. 9 Ca-Zn phase diagram

For this phase diagram, all crystallization regions of congruent compounds were not described by mathematical expressions because all seven compounds in the melt dissociate before or after the melting temperature. The congruent $CaZn_2$ compound is of greater interest. The thermodynamic data used in the calculations and the derivation of the osmotic coefficient dependency (Φ''_{on}) on the for $CaZn_2$ activity $a^L_{CaZn_2,id.}$ are as follows: ΔH_{CaZn2}=9230 J/mol, $T_{m,CaZn2}$=977 K [14], [18].

Table 11 presents the $CaZn_2$ crystallization region in the $CaZn_2$-Ca system. Let's examine the behavior of the components in the melt for the first $CaZn_2$ crystallization region in the $CaZn_2$-Ca system.

Table 11 Initial data of the $CaZn_2$ crystallization region for the partial $CaZn_2$-Ca system

T, K	x^L_{Ca}	x^S_{Ca}	$x^L_{CaZn_{2расч.}}$	$a^L_{CaZn_2}$	$\Phi'_{CaZn_{2 баз.}}$	Φ''_{CaZn_2}
977	0,333	0,333	1,002	1,000	0	0,000
973	0,388	0,333	0,789	0,995	-0,030558	0,020
948	0,43	0,333	0,663	0,966	-0,135968	0,085
923	0,445	0,333	0,624	0,936	-0,229286	0,141
898	0,46	0,333	0,587	0,905	-0,309397	0,188
873	0,474	0,333	0,555	0,873	-0,383395	0,230
848	0,485	0,333	0,531	0,841	-0,459706	0,273
823	0,496	0,333	0,508	0,808	-0,533638	0,314
798	0,513	0,333	0,475	0,775	-0,589812	0,342
773	0,524	0,333	0,454	0,741	-0,661453	0,380
748	0,54	0,333	0,426	0,706	-0,719589	0,408
716	0,57	0,333	0,377	0,661	-0,770611	0,425

According to **Table 11**, we plotted a graph (**Fig. 10**) showing the dependence of the Bjerrum-Guggenheim osmotic coefficient (Φ''_{on}) on the $CaZn_2$ crystallization activity $a^L_{CaZn_2}$ for the partial $CaZn_2$-Ca system relative to the baseline data. The Bjerrum-Guggenheim osmotic coefficient for this $CaZn_2$ crystallization region has negative values. Additionally, the dependence in **Fig. 10** is curvilinear, which means that in the melt, the curvature Φ_i is primarily influenced by the nature of the directional bonds in the associates and the change in their numerical values with temperature.

The graph of the dependence of the Φ'_{CaZn_2} on $a^L_{CaZn_2}$ exhibits weak concavity, starting from the melting temperature of $CaZn_2$. This suggests a strong interparticle interaction of the components in the melts and weak dissociation of $CaZn_2$. However, with the transition of compositions to the $CaZn_2$ crystallization region, the formation of associates occurs, as the graph of Φ'_{CaZn_2} has a concave character in this area. By processing the data using the least squares method according to the dependence of the Φ'_{CaZn_2} on $a^L_{CaZn_2}$, we obtain the dependence (18), with the calculation result δ=0.0086 (which gives a deviation from the experimental data within 0.2% abs.) for the liquid-phase of the $CaZn_2$ crystallization region.

$$\Phi_{CaZn_2-Ca} = -6{,}74 + 4{,}92a^L_{CaZn_2}/a^S_{CaZn_2} - 1{,}8/(0 - a^L_{CaZn_2}/a^S_{CaZn_2}),\ \delta=0.0086, \quad (18.)$$

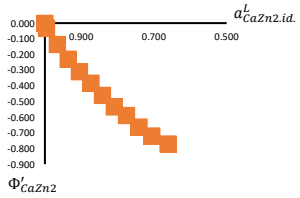

Fig. 10 The graph of the dependence of the Bjerrum-Guggenheim osmotic coefficient (Φ'_{on}) on the $CaZn_2$ crystallization activity $a^L_{CaZn2,id.*}$ for the baseline Ca-Zn system

A critical analysis of the convergence of the calculated and experimental data is presented in Table 12.

Table 12 Comparative analysis of the the calculated and experimental data for the region of $CaZn_2$ crystallization relative to the basic Ca-Zn system according to equation (18)

$\Phi''_{on.}$	$\Phi''_{расч.}$	$\ln a^L_{CaZn_2}$	$a^L_{CaZn_2}$	x^L_{Ca}/x^S_{Ca}	$x^L_{Ca}/x^S_{Ca_{расч.}}$
0,000	-0,020	0,000	1,000	1,000	1,000
-0,031	-0,036	-0,005	0,995	1,165	1,151
-0,136	-0,124	-0,035	0,966	1,291	1,326
-0,229	-0,212	-0,066	0,936	1,336	1,365
-0,309	-0,299	-0,100	0,905	1,381	1,398
-0,383	-0,383	-0,135	0,873	1,423	1,422
-0,460	-0,462	-0,173	0,841	1,456	1,454
-0,534	-0,537	-0,213	0,808	1,489	1,487
-0,590	-0,605	-0,255	0,775	1,541	1,525
-0,661	-0,665	-0,300	0,741	1,574	1,570
-0,720	-0,717	-0,348	0,706	1,622	1,624
-0,771	-0,765	-0,414	0,661	1,712	1,718

Next, the graph of the dependence of the Bjerrum-Guggenheim osmotic coefficient (Φ''_{on}) on the $CaZn_2$ crystallization activity $a^L_{CaZn_2,id*}$ for the partial $CaZn_2$-Ca system was plotted (**Fig. 11**).

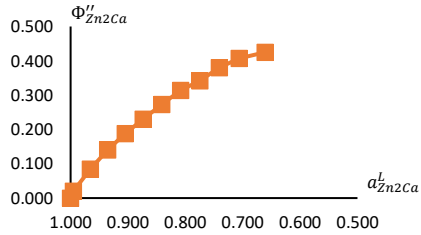

Fig. 11 The graph of the dependency of the Bjerrum-Guggenheim osmotic coefficient (Φ''_{on}) on the $CaZn_2$ crystallization activity $a^L_{CaZn_2,id*}$ for the partial $CaZn_2$ – Ca system

$$\Phi_{CaZn_2-Ca} = 4{,}623 - 3{,}254a^L_{CaZn_2}/a^S_{CaZn_2} - 1{,}36/(0 - a^L_{CaZn_2}/a^S_{CaZn_2}),\ \delta=0.0086, \quad (19.)$$

During the conversion of the compositions to the partial $CaZn_2$-Ca system, with conversion coefficients for this region equal to I=1, J=2, Q=1, and P=0, the graph depicting the dependence of Φ''_{CaZn_2} on $a^L_{CaZn_2}/a^S_{CaZn_2}$ (**Fig. 11**) for the liquid-phase region exhibits a strictly convex correlation, indicating predominantly dissociation or association processes in the melt [22] - [26]. A

comparative analysis of the calculated (19) and experimental data (Table 11) is presented in **Table 13**.

Table 13 Comparative analysis of the calculated and experimental data on the $CaZn_2$ crystallization region for the partial $CaZn_2$-Ca system according to (19)

$\Phi^{''}_{on.\,расч.}$	$\Phi^{''}_{CaZn_2\,расч.}$	$\ln a^{L}_{CaZn_2}$	$a^{L}_{CaZn_2}$	$x^{L}_{CaZn_2}$	$x^{L}_{CaZn_2\,расч.}$
0	0,014	0,000	1,000	1,002	1,000
0,02	0,023	-0,005	0,995	0,789	0,807
0,085	0,077	-0,035	0,966	0,663	0,634
0,141	0,129	-0,066	0,936	0,624	0,600
0,188	0,181	-0,100	0,905	0,587	0,575
0,23	0,230	-0,135	0,873	0,555	0,556
0,273	0,275	-0,173	0,841	0,531	0,533
0,314	0,316	-0,213	0,808	0,508	0,510
0,342	0,352	-0,255	0,775	0,475	0,485
0,38	0,383	-0,300	0,741	0,454	0,457
0,408	0,406	-0,348	0,706	0,426	0,424
0,425	0,421	-0,414	0,661	0,377	0,374

$CaZn_2$ crystallization region in the $CaZn_2$-Zn system. Employing the procedure described above, **Table 14** shows the initial data for the $CaZn_2$- crystallization region in the $CaZn_2$-Zn system with conversion factors for this region equal to I=1, J=2, Q=0 P=1.

To calculate the activity ratio in the liquid and solid phases according to (3), the following thermodynamic data were used: ΔH_{CaZn2}=9230 J/mol, $T_{mel.\,CaZn2}$= 977 K [14], [15].

Table 14 Initial data of the $CaZn_2$ crystallization region for the partial $CaZn_2$-Zn system

T,	x^{L}_{Ca}	x^{S}_{Ca}	$x^{L}_{CaZn_2\,расч.}$	$a^{L}_{CaZn_2}$	$\Phi^{'}_{CaZn_2\,баз.}$	$\Phi^{''}_{CaZn_2}$
97	0,3	0,33	0,9970	1	0	0
97	0,3	0,33	0,8888	0,9988	0,029235	0,009
97	0,3	0,33	0,8440	0,9976	0,039673	0,013
97	0,3	0,33	0,8157	0,9953	0,065267	0,022
96	0,3	0,3	0,75	0,983	0,15828	0,057
95	0,2	0,33	0,7195	0,9717	0,236164	0,086
94	0,2	0,33	0,7019	0,9658	0,264553	0,098
93	0,2	0,33	0,6520	0,9478	0,329364	0,125
91	0,2	0,33	0,6111	0,9258	0,402323	0,156

After converting gross concentrations to net concentrations, the curve of the dependence of Φ''_{CaZn_2} on $a^{L}_{CaZn_2}/a^{S}_{CaZn_2}$ clearly exhibits a convex nature, starting from the melting temperature of the chemical compound and increasing as the temperature decreases to the eutectic horizontal at 915 K, indicating an increase in the dissociation process of the congruent compound (**Fig. 12**). **Table 15** shows the convergence of the experimental concentrations with the ones calculated using (20).

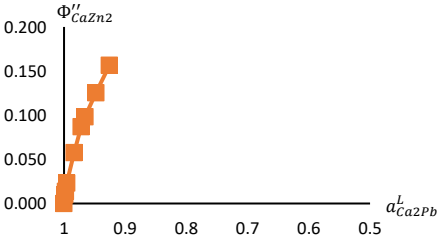

Fig. 12 The graph of the dependence of the Bjerrum-Guggenheim osmotic coefficient (Φ''_{on}) on the $CaZn_2$ crystallization activity $a^{L}_{CaZn_2,id*}$ for the partial $CaZn_2$ – Zn system

The mathematical processing of the obtained results and the comparison of the numerical values of the Bjerrum-Guggenheim osmotic coefficient (Φ''_{on}) against the activity $a^{L}_{CaZn_2,id*}$ for the experimental and calculated data were conducted using (20).

$$\Phi_{CaZn_2-Ca} = 34{,}827 - \frac{19{,}04a^{L}_{CaZn_2}}{a^{S}_{CaZn_2}} + 15{,}78\,/\,(0 - a^{L}_{CaZn_2}/\,a^{S}_{CaZn_2})\,,\ \delta{=}0.0179 \qquad (20.)$$

Table 15 Comparative analysis of the calculated and experimental data on the $CaZn_2$ crystallization region for the partial $CaZn_2$-Zn system according to (20)

$\Phi^{''}_{on.\,расч.}$	$\Phi^{''}_{CaZn_2\,расч.}$	$\ln a^{L}_{CaZn_2}$	$a^{L}_{CaZn_2}$	$x^{L}_{CaZn_2}$	$x^{L}_{CaZn_2\,расч.}$
0	0,011	0	1	0,997	1
0,009	0,01477	-0,0012	0,998	0,888	0,92424
0,013	0,01851	-0,0023	0,997	0,844	0,88170
0,022	0,02586	-0,0047	0,995	0,815	0,83477
0,057	0,06016	-0,0165	0,983	0,75	0,75992
0,086	0,09015	-0,0286	0,971	0,719	0,72804
0,098	0,10344	-0,0348	0,965	0,701	0,71460
0,125	0,13599	-0,0536	0,947	0,652	0,67432
0,156	0,15930	-0,077	0,925	0,611	0,61674

Thus, for both partial systems, i.e. $CaZn_2$-Ca and $CaZn_2$-Zn, the $CaZn_2$ crystallization regions exhibit a distinctly convex character in the graphs depicting the dependence of the Bjerrum-Guggenheim osmotic coefficient (Φ''_{on}) on the activity $a^{L}_{CaZn_2,id*}$. This indicates that within the range based on the chemical compound $CaZn_2$, solid solutions contain an excess of one of the components relative to the stoichiometric composition of the compound. Obviously, all solid solutions in the region of the intermediate phase homogeneity are unsaturated. Since the left part of the $CaZn_2$-Ca phase diagram occupies a larger area below the ordinate of the congruent compound, and therefore the substitution process is more intense, the graphs depicting the dependence of the Bjerrum-Guggenheim coefficient immediately showed that the dissociation process is ongoing, and the interaction forces between the components are changing. Taking into

account the degree of dissociation of this compound, the graphs Φ''_{CaZn_2} should exhibit a strictly correlational form [27].

CONCLUSION

Theoretical analysis of the melt structure based on the behavior of the Bjerrum-Guggenheim osmotic coefficient in the melts of the general Fe-Si-Al-Ca-Mg-Zn-Pb system showed that complex high-temperature chemical compounds with impurity elements such as zinc and lead do not form in the melt, and there are no obstacles to the high degree of volatility of these elements.

Theoretical studies have been conducted on the nature of changes in the Bjerrum-Guggenheim osmotic coefficient (positive Φ_i <1 or negative Φ_i >1 in the melt) for two binary Ca-Pb and Ca-Zn systems.

Phase diagrams of Ca-Pb and Ca-Zn are characterized by the formation of congruent compounds. The behaviour of the Bjerrum-Guggenheim osmotic coefficient for systems containing calcium shows that almost all systems exhibit positive deviation from ideality, i.e., interactions between atoms of the same type occur. Congruent compounds are characterized by a high degree of dissociation.

Acknowledgements: This research was funded by the Industrial Development Committee of Industry of the Ministry of Industry and Construction of the Republic of Kazakhstan (Grant №. BR19777171).

REFERENCES

1. V.M. Shevko, M.A. Tuleev, G.E. Karataeva, D.K. Aitkulov: International Journal of Applied and Fundamental Research, 3(10), 2016, 190-193 (in Russian). https://s.applied-research.ru/pdf/2016/10-2/10314.pdf.
2. A.M. Esengaziev, R.Kh. Sharipov, E.K. Markaev, E.N. Suleimenov: Science and World, 52(12), 2017, 49-57 (in Russian). https://www.elibrary.ru/download/elibrary_43080681_96217629.pdf.
3. V.D. Bortsov: Non-ferrous Metals, 32(6), 2004, 11-14 (in Russian). https://www.rudmet.ru/journal/1059/article/17061/.
4. E. A. Emelyanenko: *Monitoring subsystems of processing copper-pyrite deposits of the Ural type, conditions for the sustainable functioning of the mineral resource complex of Russia*, Moskow: Mining Book, 2014, Issue. 2, p. 111-132 (in Russian).
5. A. A. Antonenko, A. T. Khodzhimuratova, D. B. Tugaibayeva, Z. Zh. Nurdauletova, N. A. Medeshova: News of National Academy of Sciences of the Republic of Kazakhstan, 5(431), 2018, 190-197. https://doi.org/10.32014/2018.2518-170X.49.
6. Nayak A., M. Jena, R. Narayan: Mineral Processing and Extractive Metallurgy Review, 43(5), 2022, 1-20. https://doi.org/10.1080/08827508.2021.1903459.
7. R.K. Sharipov, U.A. Balgimbaeva, E.N. Suleimenov: Electrochemical Extraction of Pb and Zn from Raw Mineral Materials Using Sulfurgraphite Electrode, *9th International Symposium on Lead and Zinc Processing*. The Minerals, Metals & Materials Series, Springer: Cham, 2020, p. 429-435. https://doi.org/10.1007/978-3-030-37070-1_37.
8. K. S. Izbaskhanov,: KazTU Khabarshysy, 5, 2015, 311-320 (in Russian). https://vestnik.satbayev.university/index.php/journal/issue/view/24/23.
9. S.O. Baisanov, V.V. Tolokonnikova, G.I. Narikbayeva, I.Y. Korsukova, N.R. Vorobkalo: High Temperature, 60(6), 2022, 775-780. https://doi.org/10.1134/s0018151x22050194.
10. S. Baisanov, V. Tolokonnikova, G. Yerekeyeva, G. Narikbayeva, I. Korsukova: Metalurgija, 61(3-4), 2022, 828-830.
11. V.V. Tolokonnikova, S.O. Baisanov, G.I. Narikbayeva, G.S. Yerekeyeva: CIS Iron and Steel Review, 24, 2022, 79-83. https://doi.org/10.17580/cisisr.2022.02.12.
12. V.V. Tolokonnikova, S.O. Baisanov, G.I. Narikbayeva, I. Korsukova, Y. Mukhambetgaliyev: Metalurgija, 60(3-4), 2021, 292-294.
13. M. Hansen, K. Anderko: *Structure of binary alloys*. Metallurgy: Moscow, 1962, p. 556-566 (in Russian).
14. V.P. Glushko: *Thermodynamic properties of individual substances*. Directory. VINITI Institute of High Temperatures of the USSR Academy of Sciences: Moscow, 1982, p. 456 (in Russian).
15. *Scientific Group Thermodata Europe 2017* [Electronic resource] – URL: https://www.factsage.com/ (date of the application 2023–03–10).
16. R.A. Robie, B.S. Hewingway, J.K. Fisher: Thermodinamic Properties of Minerals and Related Substances at 298,15 and (105 Paskals) Pressure and Higher Temperatures, Bulletin, 1452, 1978, p. 456. https://doi.org/10.3133/b1452.
17. A.N. Krestovnikov, L.P. Vladimirov, V.S. Gulyanitsky, A.Ya. Fisher: *Handbook for calculations of equilibria of metallurgical reactions*. GNTI Literature on ferrous and non-ferrous metallurgy: Moscow, 1968, P. 416 (in Russian).
18. L.P. Ruzinov, V.S. Gulyanitsky: *Equilibrium transformations of metallurgical reactions*. Metallurgy: Moscow, 1975, p. 417 (in Russian).
19. Database http://www.outokumpu.fi/hsc [Electronic resource] /5.12.23.
20. G.L. Katkeeva, G. Burkitseterkyzy, I.M. Oskembekov, E.M. Zhunusov: Obogashchenie Rud, 3, 2020, 38–42. https://doi.org/10.17580/or.2020.03.07.
21. I.M. Oskembekov, G.L. Katkeeva: Obogashchenie Rud, 5, 2014, 51–54. https://www.rudmet.ru/journal/1352/article/23200/.
22. A.A. Akberdin, A.S. Kim, A.S. Orlov, R.B. Sultangaziev: CIS Iron and Steel Review, 1, 2022, 76-80. https://doi.org/10.17580/cisisr.2022.01.14.
23. A.A. Akberdin, A.S. Kim, A.S. Orlov, R.B. Sultangaziev, A.M. Makasheva: Metalurgija, 62(1), 2023, 49-52.
24. A.S. Kim, A.A. Akberdin, R.B. Sultangaziyev, A.S. Orlov: Metalurgija, 61(2), 2022, 305-308.
25. F.R. Kapsalamova, S.A. Krasikov, A.Z. Terlikbaeva, E.M. Zhilina, A.M. Alimzhanova: Russian Metallurgy (Metally), 2023(8), 2023, 1081–1088. https://doi.org/10.17580/tsm.2023.08.15.
26. Ye. Makhambetov, Ye. Myngzhassar, A. Abdirashit: Acta Metallurgica Slovaca, 30, 1, 2024, 29-33. https://doi.org/10.36547/ams.30.1.1998.
27. V.V. Tolokonnikova, S. Baysanov, Zh.K. Saulebek, A.S. Orlov: CIS Iron and Steel Review,2, 2023, 105-110. https://doi.org/10.17580/cisisr.2023.02.17.